Scanning Electron Microscopy

Volume 3
Number 1 *3rd Pfefferkorn Conference*

Article 13

1984

Optimization of Stroboscopic Electron Deflection Systems

H. Rose
New York State Department of Health

J. Zach
Technische Hochschule Darmstadt

Electron Optical Systems (pp. 127-135)
SEM Inc., AMF O'Hare (Chicago), IL 60666-0507, U.S.A.

0-931288-34-7/84$1.00+.05

OPTIMIZATION OF STROBOSCOPIC ELECTRON DEFLECTION SYSTEMS

H. Rose* and J. Zach†

Center for Laboratories and Research
New York State Department of Health
Albany, NY 12201
and
†Institut für Angewandte Physik
Technische Hochschule Darmstadt
D-6100 Darmstadt, FRG

Abstract

Highly corrected electron-beam blanking systems (EBBS) are required for analyzing fast periodic processes at submicron spatial resolutions by stroboscopic methods. The deleterious degradation of the probe during the blanking operation can be avoided by a new straight-vision deflection system. Chopping of the beam is performed within this system by deflecting it across a knife edge. Calculations demonstrate that this system should be able to generate almost rectangular beam pulses with rise times of a few picoseconds and spot sizes smaller than 0.5 μm. The proposed EBBS consists of two wedge-shaped plate capacitors located symmetrically about the midplane of a rotationally symmetric double lens. Time-of-flight effects are largely compensated by driving the two capacitors as a traveling-wave structure to yield resonance deflection.

KEY WORDS: Electron-beam blanking systems, electron stroboscopy, resonance deflection, aberration correction, oblique plate capacitor, time-of-flight effects, temporal resolution, spatial resolution.

*Address for correspondence:
H. Rose, Inst. fur Angew. Physik
T.H. Darmstadt, D-6100 Darmstadt, FRG
Phone No.: 6151-162481

Introduction

Electron-beam blanking systems (EBBS) are increasingly used as basic devices in electron lithography and electron-beam testing systems and for measurement of time-dependent, spatially localized processes in thin specimens. For each application the EBBS must meet different requirements with respect to pulse width, repetition rate, beam current, and accelerating voltage. Pulsed electron beams can be generated by (a) modulation of the Wehnelt voltage at the electron gun [7,12,15], (b) rotationally symmetric cavities [9] or filter lenses [10], or (c) beam deflection across a chopping aperture or a knife edge [3,4,6,8,11]. Owing to its simplicity the last approach is widely employed in stroboscopically operating scanning electron microscopes (SEM). These instruments are increasingly used for functional testing of integrated circuits by voltage-contrast measurements. This method enables one to visualize periodically changing potentials, either for a constant phase position (by scanning the beam over the surface of the specimen) or as a function of phase (at a fixed position in the circuit) [1,2].

High time resolution necessitates electron pulses with very short rise times. Furthermore, to prevent falsification of the signal, both the position and the size of the scanning spot at the specimen should be as unaffected by the blanking operation as possible. Investigation of emitter-coupled logic chips and GaAs circuits in the near future, for example, will require almost rectangular pulses of widths between 50 ps and 5 ns and stable spot sizes smaller than 0.5 μm [6]. These requirements cannot be fulfilled with presently used deflection blanking systems consisting of a single capacitor. Therefore we shall investigate in this paper EBBS composed of more than one capacitor together with static magnetic round lenses. These lenses may belong to the SEM or may be incorporated separately into the EBBS. Furthermore we shall impose no restrictions on the geometry of the deflection system except that its fields can be considered as two-dimensional in the region of the electron beam. Magnetic deflection coils will not be considered because they are not suitable for obtaining very fast deflections.

Quasistatic Field Approximation

The propagation of electrons in fast time-varying deflection fields has received little attention in theoretical electron optics. However, the standard stationary treatment is no longer applicable when the fields change significantly during the passage of the electrons through an EBBS. In this case time-of-flight effects influence the electron path and must therefore be taken into account.

Let us restrict our considerations to signals whose dominant frequencies are small compared to c/L where c is the velocity of light and L is the length of the EBBS in the direction of the beam. With this assumption the electric fields can be considered as quasistatic. This approximation assumes that the magnetic vector potential $\vec{A}$ does not explicitly depend on the time variable t, so that $\partial\vec{A}/\partial t = 0$, which means that the effects of the magnetic fields produced by the time-varying electric fields are negligibly small. As a result both the electric field $\vec{E}$ and the magnetic flux density $\vec{B}$ outside the region of the conductors and currents can be obtained from scalar potentials $\phi = \phi(\vec{r},t)$ and $\psi = \psi(\vec{r})$ respectively:

$$\vec{E} = -\text{grad}\ \phi, \qquad \vec{B} = -\text{grad}\ \psi. \tag{1}$$

Assume further that the capacitors can be considered as infinitely extended in the y direction perpendicular to the straight optic axis, which is chosen as the z axis of the Cartesian coordinate system. Because the electric signal applied to the capacitors travels in the y direction and because the diameter of the electron beam is small compared to the wavelengths of the plane-wave components of the signal, the electric potential in the region of the beam can be written as:

$$\phi(\vec{r},t) = \Phi_D(x,z)g(t) + \bar{\Phi} + \delta\Phi\ . \tag{2}$$

Here $\bar{\Phi}$ is the constant axial potential at a large distance from the deflection system; $\delta\Phi$ is the deviation due to the energy spread of the emitted electrons; and:

$$\Phi_D(x,z) = \Delta + \Phi_1 x - \Delta'' x^2/2 - \Phi_1'' x^3/6 + \ldots \tag{3}$$

is the static potential of a two-dimensional capacitor. Dashes represent derivatives with respect to the z coordinate; $\Phi_1 = \Phi_1(z)$ is the strength of the dipole field, while $\Delta = \Delta(z)$ represents the deviation of the axial potential from the anode potential . This deviation vanishes only if the plates of the capacitors are arranged symmetrically about the plane x = o and are excited antisymmetrically, so that one plate is at the potential $\phi_D = U$ and the other at $\phi_D = -U$ with respect to ground. A nonrealistic example of such a capacitor, consisting of two inclined plates, is shown in Fig. 1. The plates intersect at the line x = o, $z = z_0$ and enclose an angle 2θ. In the case of antisymmetric excitation the potential is

$$\phi_D = (U/\theta)\arctan[x/(z-z_0)] \approx (U/\theta)[x/(z-z_0) - x^3/3(z-z_0)^3 + \ldots] \tag{4}$$

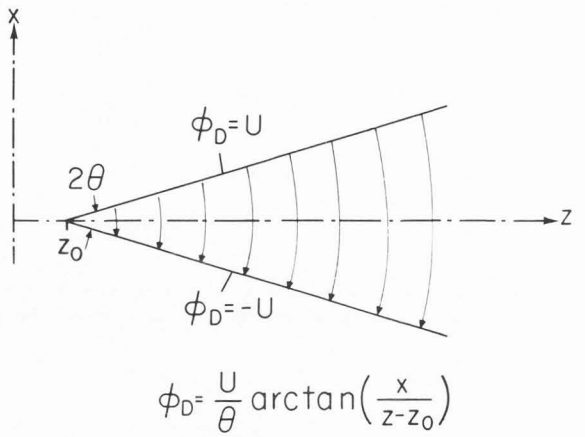

Fig. 1. Electric-field distribution in the region between two inclined half-planes at potentials $\phi_D = U$ and $\phi_D = -U$.

The lines of constant electric field are circles about the origin $z = z_0$, x = o. If we neglect the fringing fields, relation (4) also describes approximately the electric field within a real capacitor with inclined plates, provided their extension is large compared to the maximum gap width.

In the expansion (3) the terms which comprise the axial potential and its derivatives represent the potential expansion of a cylinder lens. Hence any asymmetrically excited capacitor can be considered as a linear superposition of a cylinder lens and a deflection field whose potential is antisymmetric with respect to the midplane x = o. The time-varying cylinder lens acts like a buncher.

Upon introduction of the complex off-axial coordinates:

$$w = x + iy,\ \bar{w} = x - iy \tag{5}$$

the power series expansion of the scalar magnetic potential of the round lenses has the form:

$$\psi = \Psi - (w\bar{w}/4)\Psi'' + \ldots \tag{6}$$

where $-\Psi' = B_0$ is the magnetic flux density along the symmetry axis.

Equations of Motion

The equations for describing electron motion in time-dependent fields can be obtained either from the Lagrangian, as outlined by Sturrock [13], or by employing Newton's law together with the Lorenzian expression for the electromagnetic force acting on the electrons. Assuming $\vec{A} = 0$ with nonrelativistic electron velocities, we eventually arrive after some manipulations at the following equations:

$$m(w'/t')' = e\left\{2t'\frac{\partial\phi}{\partial\bar{w}} + 2i\frac{\partial\psi}{\partial\bar{w}} - iw'\frac{\partial\psi}{\partial z}\right\}, \tag{7}$$

$$E' = \frac{m}{2}\left(\frac{1+w'\bar{w}'}{t'^2}\right)' = e\left\{\frac{\partial\phi}{\partial z} + 2\,\text{Re}\left(\bar{w}'\frac{\partial\phi}{\partial\bar{w}}\right)\right\}. \tag{8}$$

Here e, m, and $1/t' = v_z$ denote the charge, mass, and axial velocity component of the electron respectively. Its kinetic energy $E = E_z + E_w$ consists of an axial component:

$$E_z = mv_z^2/2 \tag{9}$$

and a transverse component:

$$E_w = mw'\bar{w}'/2t'^2. \tag{10}$$

The solution $w = w(z)$, $t = t(z)$, of the nonlinear coupled differential equations (7,8) is an implicit representation of the electron position as a function of time. The right-hand side of the temporal equation (8) is a total differential with respect to z only if the electric potential does not depend on time. Then the z integration can be performed readily to yield a constant total energy. This well-known result, however, no longer holds true in the case of a time-varying potential.

The system (7,8) of nonlinear differential equations can be solved approximately by means of well-established perturbation methods. For this purpose we write

$$t(z) = T(z) + \tau(z) , \tag{11}$$

where T denotes the time taken by an electron traveling along the axis when the deflection system is switched off. Accordingly τ is the time difference for an electron not moving along this straight axis to reach the same plane. In a zeroth-order approximation we derive from (8):

$$T' = (m/2e\Phi)^{1/2} = \text{const.} , \quad \tau^{(0)} = 0, \tag{12}$$

which corresponds to $E^{(0)} = E_z^{(0)} = E_o = e\Phi = mv_o^2/2$. Here v_o and E_o are the initial average velocity and the mean kinetic energy respectively of the electrons below the anode. Within the frame of our approximation procedure we consider $w, \bar{w}, w', \bar{w}', \tau, \Phi_1, \delta\Phi$ and Δ to be small quantities.

Dynamic Gaussian Dioptrics

The first-order equations are obtained from (7,8) by retaining only those terms which are linear in the expansion parameters. The resulting dynamic paraxial equations

$$w^{(1)''} - 2i\chi' w^{(1)'} - i\chi'' w^{(1)} = g(T)D(z) , \tag{13}$$

$$E^{(1)} = E_z^{(1)} = -m\tau^{(1)'}/T'^3 = e\int_{z_i}^{z}\Delta' g\,dz + e\delta\Phi \tag{14}$$

take account to a first approximation of time-of-flight effects, since they replace the local distributions $D(z) = \Phi_1/2\Phi$ and Δ of the deflection field by the effective fields $g(T)D$ and $g(T)\Delta$ respectively, as seen by an electron traveling along the axis with the initial axial velocity v_o. The angle:

$$\chi = (e/8m\Phi)^{1/2}\int_{z_i}^{z} B_o\,dz \tag{15}$$

describes the Larmor rotation of an electron starting from the initial plane z_i. Also:

$$T = (z - z_i)/v_o \tag{16}$$

is the time an electron needs to travel from this plane along the axis to plane z.

The first-order time equation (14) convincingly demonstrates that the so-called temporal aberrations [5] are closely connected with changes in the kinetic energy of the electrons. This energy deviation is caused by the energy spread of the emitted electrons and by the time-varying part of the electric potential. Expressing the time T in the time function by relation (16), we find from (14) that, within the frame of the first-order approximation, the kinetic energy lost or gained by the electron when passing through the asymmetrically driven capacitor is proportional to the convolution of the time function and the static axial field $-\Delta'$. To survey this energy change we assume a step pulse:

$$g(T) = \begin{cases} 0 \text{ for } T \le T_o = (z_o - z_i)/v_o \\ 1 \text{ for } T > T_o \end{cases} \tag{17}$$

This choice implies that the capacitor is switched on instantaneously when the electron is at plane z_o. With this relation the integration in (14) can be performed readily, yielding:

$$E^{(1)} = \begin{cases} 0 \text{ for } z \le z_o \\ e(\Delta - \Delta_o) \text{ for } z > z_o \end{cases} \tag{18}$$

where $\Delta_o = \Delta(z_o)$. In the opposite case where the capacitor is switched off, we find:

$$E^{(1)} = \begin{cases} e\Delta \text{ for } z \le z_o \\ e\Delta_o \text{ for } z > z_o \end{cases} . \tag{19}$$

The comparison shows that at a large distance from the capacitor, where $\Delta = 0$, the electron has lost the kinetic energy $e\Delta_o$ in the former case, while it gains the same amount if the capacitor is off. This difference in behavior occurs because the kinetic energy of the electron remains unchanged when the potential jumps. In the former case the electron loses kinetic energy when it leaves the capacitor because the potential Δ decreases in the exit region slowly toward zero. When the capacitor is switched off abruptly, the electron retains the kinetic energy which it has gained by entering regions of steadily higher potential within the capacitor. In practice the kinetic energy is changed significantly only when the transit time of the electron through the blanking system is large compared to the rise time of the pulse during the passage. No such first-order energy change occurs when the capacitor is driven in such a way that the potential in the midplane remains equal to the constant anode potential.

It is convenient to express the Gaussian rays in the rotating coordinate system:

$$u = we^{-i\chi} . \tag{20}$$

Then the general solution of the paraxial path equation (13) has the form:

$$u^{(1)} = u_C u_\gamma + \omega_A u_\alpha + u_\delta . \tag{21}$$

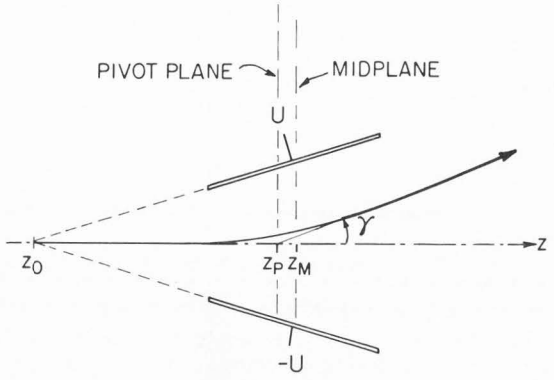

Fig. 2. Beam deflection by a wedge-shaped plate capacitor; γ denotes the deflection angle.

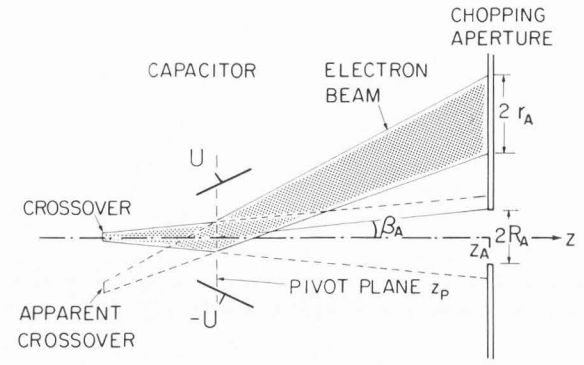

Fig. 3. Scheme of electron-beam blanking by a single plate capacitor placed between the crossover and the effective (final) chopping aperture.

The term

$$u_\delta = u_\gamma \int_{-\infty}^{z} g D e^{-i\chi} u_\gamma \, dz - u_\gamma \int_{-\infty}^{z} g D e^{-i\chi} u_\alpha \, dz \qquad (22)$$

represents the deflection of the beam. The real functions u_α and u_γ are linearly independent solutions of the homogeneous part (D = 0) of (13) which satisfy the boundary conditions:

$$\begin{aligned} u_\gamma(z_A) &= u_{\gamma A} = u_\alpha(z_C) = 0, \\ u_\gamma(z_C) &= u_\alpha'(z_A) = 1 \quad . \end{aligned} \qquad (23)$$

Here z_C and z_A denote either the locations of the crossover and the final beam-limiting aperture respectively or the locations of their intermediate images; and $|u_C|$ and $u_{\alpha A}$ $|\omega_A| = |u_A|$ are the radii of the crossover and of the final beam-limiting aperture at the corresponding planes.

To survey the action of a dipole field on the beam we evaluate (22) in the absence of overlapping round lenses and for a single capacitor with inclined plane plates, as shown in Fig. 2. In this case we have $\chi = 0$ and $g = 1$. Using the expansion (4) for the deflection potential together with (3) and neglecting the fringing fields, we find:

$$D = \pm U/[2(z-z_0)\theta\Phi] \qquad (24)$$

The sign is plus when z_0 is on the left side of the capacitor and minus when z_0 is on the right. If we insert this expression into (22), the integration can be performed analytically to yield the following expression for the deflection in the region below the capacitor:

$$u_\delta = w_\delta = (z-z_p)\gamma \qquad (25)$$

where

$$\gamma = (U/2\theta\Phi)\ln(1+l/s) \qquad (26)$$

is the deflection angle;

$$z_p = z_0 \pm l/\ln(1+l/s) \qquad (27)$$

denotes the location of the pivot plane, s is the distance between z_0 and the capacitor, and l is the length of the capacitor. Here the sign is plus when the intersection z_0 of the extended plates is in front of the capacitor, viewed in the direction of the axis; the sign is minus in the opposite case. For a wedge-shaped capacitor the pivot plane z_P does not coincide with the midplane z_M, as in the case of a parallel plate capacitor, but is shifted toward the intersection point z_0.

Degradation of Spatial Resolution by Blanking

Beam pulses are generated by deflecting the beam across the hole of a chopping diaphragm or across a knife edge. In most instruments the beam-limiting diaphragm in the final lens is used for chopping. The EBBS is usually placed above or below the first lens, because the virtual image of this diaphragm is very small in this region. The final image, located at a plane z_A below the EBBS is an effective chopping aperture, as electrons which do not pass through this aperture are removed from the beam by the final diaphragm.

The blanking operation is generally connected with an apparent movement of the crossover, as shown in Fig. 3. The corresponding displacement $u_{\delta S} = u_\delta(z_S)$ of the probe at the specimen plane z_S causes an enlargement of the probe size and hence a degradation of spatial resolution. We define the degradation:

$$\delta = |u_{\delta S}|/(u_{\gamma S}|u_C|) = |u_C|^{-1} \int_{-\infty}^{z_S} I(z)dz \qquad (28)$$

as the ratio of beam displacement to the radius $u_{\gamma S}|u_C|$ of the real probe at the specimen plane. Here:

$$I(z) = g(T) D e^{-i\chi} u_\alpha \quad . \qquad (29)$$

The spot remains at rest during blanking only if the degradation vanishes. This occurs, for example, if the integrand (29) on the right-hand side of (28) is antisymmetric with respect to a certain plane of the EBBS. It has often been stated that the degradation would vanish if the center of gravity of the deflection field D were placed at an intermediate image of the crossover. However, this conjecture holds true only for the static situation (g = 1) or for an infinitely short deflection structure. In the real case of an extended EBBS time-of-flight effects may cause a substantial degradation when the deflection voltage changes significantly during the transit time of the electrons. This behavior becomes more obvious

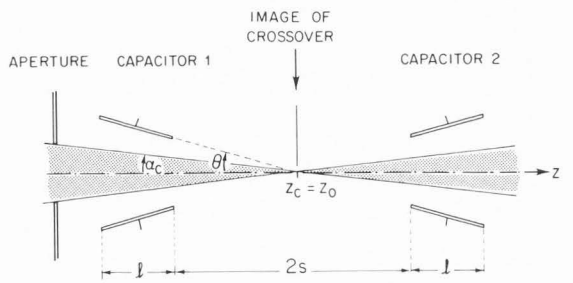

Fig. 4. Deflection structure consisting of two wedge-shaped plate capacitors positioned symmetrically about an image of the crossover.

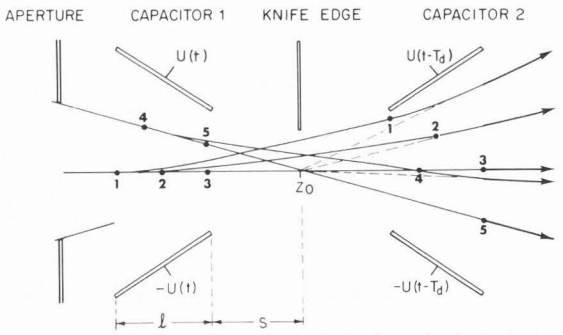

Fig. 5. Scheme of resonance beam deflection, employing the deflection structure shown in Fig. 4. The signal at the second plate capacitor is delayed by the time $T_d = (\ell + 2s)/v_o$, where v_o is the velocity of the electrons. The numbers represent the two positions of each different electron as it passes through the first and second capacitor when the deflection voltage is switched on. The dashed lines indicate the asymptotes of the emergent electron trajectories.

if we consider that electrons within the capacitor will pivot on different planes when the deflection voltage is changed abruptly, depending on their instantaneous axial positions.

In the case of a fast time-varying deflection voltage the integrand (29) cannot be made antisymmetric with respect to the midplane z_M of the deflection structure. Fortunately the degradation also vanishes if the integrand fulfills the conditions:

$$I(z+b) = -I(z) \quad , \quad 0 \le z_M - z \le b \, , \tag{30}$$

where b+l is the total length of the deflection system. This requirement can be met by placing two wedge-shaped capacitors separated by a distance 2s symmetrically about an intermediate image $z_C = z_M$ of the crossover. Such an arrangement is depicted schematically in Fig. 4. The plates are inclined in such a way that their elongations intersect each other at the crossover ($z_O = z_C$). In this case the factor $Du_\alpha \exp(-i\chi)$ is antisymmetric with respect to the midplane and constant within each capacitor. This behavior follows if we use expression (24) together with $u_\alpha = z - z_O$ and remember that χ is constant in the absence of magnetic fields at the deflection system. Hence condition (30) is fulfilled if the time function has the property:

$$g[T(z+b)] = g[T(z)] \tag{31}$$

where $b = 2s + \ell$.

For this purpose we must delay the deflection signal at the second capacitor by the time $T_d = b/v_o$ with respect to the first capacitor. This delay time corresponds to the transit time of the electrons through each half of the deflection system. The delay time can be adjusted conveniently by connecting the capacitors by a wave guide of proper length. Then we obtain a so-called traveling-wave deflection structure, which has the property that each electron passes conjugate segments of the two capacitors at equal phases of the deflection voltage. As a result all electrons seem to pivot on the midplane, regardless of their initial position when the signal is switched on or off. This behavior is demonstrated more convincingly in Fig. 5, where the numbers indicate the positions of various electrons during passage through the first and second capacitor when the signal is switched on.

Temporal Resolution

Plate capacitors can be used for stroboscopically operating EBBS only if the transit time of the electrons through the deflection field is small compared to the pulse repetition rate. For accelerating voltages higher than about 1 kV and capacitor lengths in the centimeter range, the repetition frequencies must be lower than 100 MHz. Higher frequencies in the GHz region will not be considered here because they require the use of traveling-wave structures or reentrant cavities [14]. Nevertheless the rise times of the electric pulses may be in the picosecond range, depending on the shape of the pulses, which need not be sinusoidal [6].

Chopping of the beam is usually performed by a dc-biased deflector, so that the beam is normally off. The beam pulse is generated by dropping the beam into the chopping aperture, as sketched in Fig. 3. The velocity of the deflection at this plane is obtained from (19) by partial differentiation with respect to T to yield:

$$\dot{u}_{\delta A} = u_{\alpha A} \int_{\infty}^{z_A} D\dot{g} e^{-i\chi} u_\gamma dz \quad . \tag{32}$$

This relation shows that the deflection velocity of the beam is proportional to the convolution of the velocity of the driving voltage and the deflection field times a factor $u_\gamma \exp(-i\chi)$. This convolution is a function of the position of the electron at a given time. To clarify this statement let us consider a single parallel-plate capacitor which is driven by a step pulse (17). Its derivative with respect to time is $\dot{g} = v_o \, \delta(z - z_o)$, where z_o is the position of the electron when the pulse is switched on, and $\delta(z)$ is the delta function. If we insert this relation into (32), assume $\chi = o$, and remember that in the absence of round lenses the fundamental rays are straight trajectories, we eventually obtain:

$$\dot{u}_{\delta A} = (z_A - z_O) v_o D(z_o) \quad . \tag{33}$$

If we further suppose that the throw $z_A - z_P$ is large compared to the capacitor length ℓ, and to $z_P - z_O$, we find for the angular deflection velocity

$$\dot{\gamma} = \gamma F(z_o)/\tau_t = (Uv_o/d\Phi)F(z_o) \quad . \tag{34}$$

Here 2U and d are the voltage and the distance between the capacitor plates respectively; $\tau_t = \ell/v_o$ is the transit time of the electrons through the capacitor; and $F(z)$ is the normalized distribution of the deflection field along the z axis. If chopping is performed at an intermediate image of the crossover the fundamental rays u_γ and u_α must be exchanged in (32). However this exchange does not alter relation (34). If we neglect the fringing fields, F represents a box function which is unity inside and zero outside the capacitor, and γ is the maximum deflection angle. Hence in the case of a step pulse the deflection velocity conceived as a function of time differs from zero only during the period τ_t.

Next consider the other extreme situation, where the driving voltage is a slowly varying function during the transit time τ_t. In this case the resulting angular deflection velocity:

$$\dot{\gamma} = \gamma \dot{g} \tag{35}$$

varies synchronously with the driving voltage.

We define the time resolution limit τ_r as the rise time of the probe current at the specimen plane from zero to maximum intensity. This time is roughly given by the relation:

$$\tau_r = 2\beta_A/\dot{\gamma}_C \tag{36}$$

provided that the angular deflection velocity $\dot{\gamma}_C$ does not change significantly while the beam is traversing the knife edge at the chopping aperture. The angle:

$$\beta_A = [R_A + r_A - |R_A - r_A|]/2(z_A - z_P) \tag{37}$$

in Fig. 3 is determined by the smaller of two radii, either the beam radius r_A at the chopping plane or the radius R_A of the chopping aperture. Relation (36) states that the temporal resolution $1/\tau_r$ will be improved as the angle decreases and as the angular deflection velocity increases. Expressions (34) and (35) show that a high deflection velocity can be achieved if the rise time of the driving voltage is in the range of the transit time τ_t and if the electric field strength is as high as possible.

Small angles β_A can be obtained in two ways: by placing the EBBS in the region of the gun where the effective chopping aperture is very small; or by blanking the beam across a knife edge placed at the strongly demagnified intermediate image of the crossover above the final lens. The use of a field-emission gun further decreases the size of the crossover and hence the angle β_A.

Correction of Blanking Aberrations

The EBBS generates time-varying aberrations at the specimen plane which degrade the probe. In practice the main degradation stems from the displacement of the scanning spot. This zeroth-order aberration cannot be eliminated or significantly reduced by the stigmator used for astigmatism control. Although this stigmator can always be adjusted to produce a circular spot, its resulting diameter will not be appreciably smaller than the original displacement, contrary to statements found in the literature [e.g. 3,14].

To achieve high spatial resolution the beam should be pivoted on an intermediate image of the crossover. Then the displacement vanishes, as has been discussed in detail in the section on degradation of spatial resolution. The residual blurring of the probe arises primarily from two effects:

(a) The total energy of the electrons is not conserved in time-varying fields. Accordingly the energy width of the beam is broadened and further increases the chromatic aberration.

(b) The deflected beam intersects the subsequent round lenses at increasingly larger off-axial distances. This combination of the large deflection, with the defects of the final lens generates strong aberrations at the specimen plane. The direct aberrations of the deflection fields at this plane are negligibly small if the crossover at the EBBS is appreciably demagnified by the subsequent round lenses.

Diminution of chromatic aberration

The chromatic aberrations are ultimately connected with the delay time:

$$\tau = \int_{z_i}^{z} (t' - 1/v_o)\,dz \quad . \tag{38}$$

This temporal deviation occurs when the electrons change their flight directions (directional delay) and/or when their total energy is altered by either a time-varying field or the emission process (chromatic delay). Within the frame of the first-order approximation the delay time $\tau^{(1)}$ (14) is entirely chromatic and is produced by the axial component of the time-varying field and the initial energy spread. The corresponding energy change depends on the axial position of the electron at a given point of time or, from a different point of view, on the phase of the time-varying signal. Hence the overall effect of the different phases is a broadening of the energy width of the beam.

Each asymmetrically driven capacitor acts as a combination of a pure deflection element and a cylinder lens. Primarily the time-dependence of this lens causes a significant energy-broadening of the beam when the pulse rise times are of the order of the transit time of the electrons. The cylinder lens also introduces a defocus and an astigmatism at the specimen plane, because such a lens refracts the rays toward its midplane.

These deleterious defects can be avoided if the capacitor plates are excited antisymmetrically so that the midplane remains at anode potential ($\Delta = 0$). This is achieved in practice (e.g. in television sets) by using two perfectly symmetrical electrical supply units with the same midpoint. Assuming this driving mode ($\Delta = 0$), we obtain for the remaining primary chromatic aberration the expression:

$$u_{cS}^{(2)} = (\delta\Phi/\Phi)C_c^{(0)} \quad . \tag{39}$$

Here:

$$C_c^{(0)} = u_{\gamma S}\int_{-\infty}^{z_S} u_\alpha \{u_\delta[\chi'^2 - i(\chi' u_\delta^2)'/2u_\delta^2] - Dge^{-i\chi} - (z-z_i)g'De^{-i\chi}/2\}dz \qquad (40)$$

defines the constant of the zeroth-order chromatic aberration or, from another viewpoint, of the dispersion. Within the frame of our approximation this zeroth-order chromatic aberration is a second-rank aberration: it is bilinear in the chromatic deviation and the deflection field yet independent of the boundary (Seidel) parameters of the beam. The first term of the dispersion (40) results from the beam deflection and the unavoidable chromatic aberration of the subsequent round lenses. When the displacement is compensated, this term is found to be $\gamma C_c/M$, where C_c is the chromatic aberration constant of the final lens and $M = u_{\gamma S}$ is the magnification of the subsequent round lenses. The second term in (40) simply represents the displacement of a quasistatic deflection field. This term is zero when the pivot plane coincides with an intermediate image of the crossover. The third term, which contains the derivative of the time function g(T), allows for the fact that electrons whose velocities differ from the average axial velocity v_o intersect a given plane at slightly different times. During each time interval the deflection field at this plane changes somewhat, so the electrons are deflected differently.

The contribution of the last two terms to the dispersion is proportional to the magnification of the crossover produced by the lenses beyond the EBBS. Hence in the case $M \ll 1$ and $\gamma \neq 0$ the dispersion (40) is primarily determined by the first term, which represents a combination aberration. To avoid this most deleterious aberration, chopping must be performed within a so-called omega deflection system, which produces a bent ray-path with parallel directions for the incident and emergent electrons. Such a straight-vision system represents the electron-optical analog of the well-known Dove prism in light optics. In such a system all but the last term in (40) vanish.

Secondary temporal deviation

The delay time $\tau^{(1)}$ obtained in the first step of the approximation procedure (14) is caused entirely by the initial energy spread in the case $\Delta = 0$. The secondary temporal deviation $\tau^{(2)}$ is derived from (8) in the second step of the approximation to yield:

$$\frac{\tau^{(2)\prime}}{T'} = -\frac{E_z^{(2)}}{E_o} = \frac{E_w^{(2)}}{E_o} + \frac{E_p^{(2)}}{E_o} - \frac{E_t^{(2)}}{E_o}. \qquad (41)$$

Here:

$$E_w^{(2)}/E_o = w^{(1)\prime}\bar{w}^{(1)\prime}/2 \qquad (42)$$

represents the normalized off-axial kinetic energy in the paraxial approximation, and:

$$E_p^{(2)}/E_o = -g(T)Dx^{(1)} \qquad (43)$$

is the change of the potential energy if the electron is at an off-axial position $x^{(1)}$ within the deflection field. These two spatial terms do not vanish in the static case g = 1. They account for the different flight times of monoenergetic electrons traveling in different directions to reach the same plane. The third term:

$$E_t^{(2)}/E_o = -(3/2)(\delta\Phi/\Phi)^2 - \int_{z_i}^{z} Dg'x^{(1)}dz \qquad (44)$$

is chromatic, since it results from the change of the total energy. Here the first term on the right-hand side arises from the initial energy spread, while the second term accounts for the energy gained or lost by the electron at a fixed position when the electric field changes its strength. The chromatic aberrations generated by the secondary time deviation $\tau^{(2)}$ are of third rank and are negligibly small in the case of a straight-vision EBBS.

Third-order geometric aberrations

Apart from the chromatic aberration the spot size is limited by the third-order geometric aberrations. These aberrations consist of the third-order deflection aberrations of the EBBS, the third-order aberrations of the magnetic round lenses, and a combination aberration resulting from the beam deflection and the defects of the round lenses. The combination aberration has the form of an axial coma and may become quite large in the absence of a beam-limiting aperture at the last lens. The third-order geometric aberrations generated by the EBBS are negligibly small if the crossover there is demagnified by the subsequent lenses. In the case of the straight-vision EBBS or if a beam-limiting aperture is placed at the last round lens, the probe size is affected only by the third-order spherical aberration and the chromatic aberration of this lens and by the diffraction at the effective beam-limiting aperture.

Outline of a High Performance Blanking System

Chopping of the beam at an intermediate image of the crossover is most feasible in the region above the final lens, where the crossover is strongly demagnified. However, beam-blanking in this region by a single capacitor strongly displaces the probe. This degradation can be avoided by incorporating two capacitors which are driven in such a way that the virtual crossover between them remains at rest during the blanking operation, yet the emanating rays are strongly deflected away from the axis, as demonstrated in Fig. 5. The beam-limiting diaphragm should therefore not be placed in the final lens, because this diaphragm also chops the beam and unduly increases the rise time of the beam pulse. If the diaphragm is removed, however, the strong deflection, in combination with the unavoidable chromatic and spherical aberrations of the subsequent round lenses, produces a strong dispersion and a large axial coma, which significantly deform the probe during blanking.

The highly corrected EBBS outlined in Fig. 6 avoids these disadvantages. This Ω-deflection system consists of two identical round lenses and two oblique plate capacitors, one located above, the other below the round lenses. The pivot planes of the capacitors are at focal planes of the round lenses. An intermediate image of the crossover is located at the symmetry plane midway between these

lenses. At this plane is placed a knife edge which chops the beam. The elongations of the plates intersect at intermediate images at equal distances above and below the midplane.

Because the system incorporates two round lenses, the second capacitor compensates for the deflection and some aberrations of the first capacitor, provided that the second capacitor is driven with the appropriate time delay. To guarantee that the deflection vanishes below the EBBS the focal length $f_1 = f_2 = f$ of the two lenses must be sufficiently large to prevent overlap of their magnetic fields with the electric deflection fields. Then the course of the Gaussian rays in front of the final lens is not affected by the blanking procedure.

The capacitors must be rotated with respect to each other about the optic axis by the angle of the Larmor rotation of the magnetic round lenses. This rotation vanishes if the coil currents have opposite directions for the two lenses.

Installation of the proposed EBBS in a SEM increases its column length. The extent of this increase depends on the required demagnification of the crossover at the chopping plane z_C. Since the axis of the deflected beam is parallel to the optic axis between the two round lenses, we have $\beta_A = r_C/f$, where r_C is the radius of the demagnified crossover.

To survey the performance of the proposed EBBS let us presuppose that the currents are sufficiently low that broadening of the probe by the Boersch effect can be neglected. In this case angles $\beta_A \approx 10^{-5}$ are attainable. If we further assume driving pulses with rise times in the range of the transit time of the electrons through a single capacitor and if we use the formula (36) together with (34) and (37), we find that it should be possible to generate beam pulses whose rise times are smaller than 1 ps.

In the case of low beam voltages the magnetic round lenses between the capacitors can be replaced with electrostatic round lenses. This substitution simplifies the mechanical setup considerably, because the two electrostatic lenses can be designed as immersion lenses. Since these lenses must be identical, their fields can be generated by three spatially separated coaxial cylinders where the potentials of the outer cylinders are at ground. Then the two immersion lenses resemble a thick electrostatic einzel lens with an extremely extended inner electrode.

The chopping aperture (or knife edge) at the center of this lens must be kept at the potential of the central electrode. Since the focal length of the two lenses is large compared to both the diameter of the cylinders and their separation distances, the thin-lens approximation can be used for the actual design.

During the blanking operation the probe remains roughly at rest at the specimen plane, apart from a small residual chromatic displacement. The time-dependent dispersion constant $C_c^{(0)}$ of this zeroth-order chromatic aberration is always smaller than $2M\gamma\ell\,(1 + s/\ell)^2$ for the proposed system (Fig. 6). As an example assume a capacitor length $\ell = 1$ cm a separation distance $2s = 6$ cm, a maximum deflection angle $\gamma \approx 10^{-2}$, and a final magnification $M = 0.1$ to yield $C_c^{(0)} \approx 30$ µm. Even at low beam voltages of several kV the maximum probe displacement during blanking will remain less than about 30nm. This displacement is small compared with the spot sizes used in electron-beam testing systems.

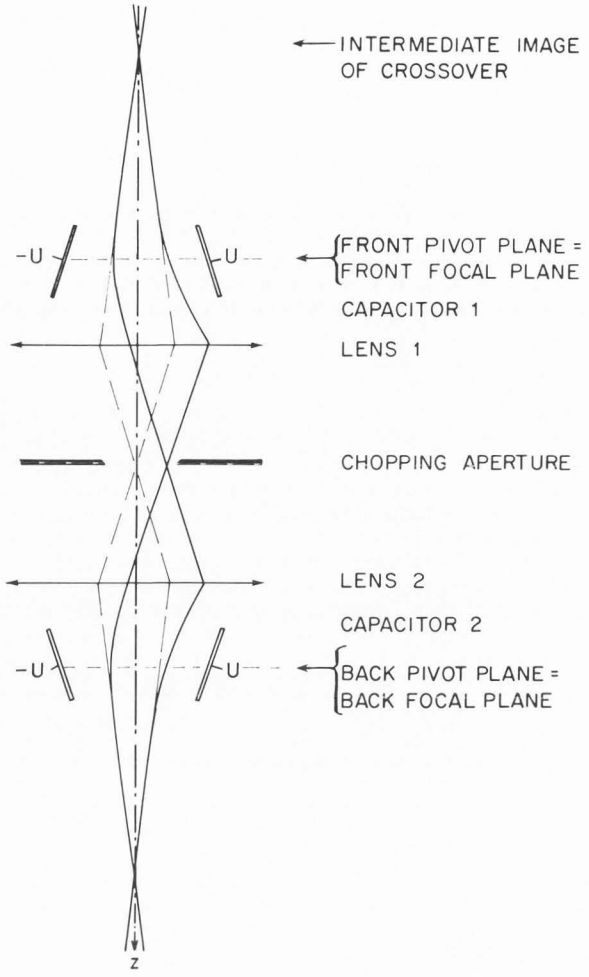

Fig. 6. Ray path in a symmetric straight-vision EBBS with an intermediate image of the crossover at the chopping aperture in the cases $U = 0$ (- - -) and $U \neq 0$ (———).

Conclusions

High-resolution electron-beam blanking can be achieved by using two oblique plate capacitors which are driven in such a way that they form a traveling-wave structure. Chopping of the beam is performed either by placing a relatively simple deflection structure (Fig. 4) at the first intermediate image of the gun crossover or by incorporating a more sophisticated straight-vision EBBS (Fig. 6) in the region of a strongly demagnified image of the crossover near the final lens of the SEM. The latter system, consisting of two capacitors and two identical round lenses, yields the highest spatial and temporal resolution, but its incorporation into the SEM extends the column length. Both blanking systems avoid probe movement, even in the case of very short pulses,

because time-of-flight effects are compensated. The proposed blanking systems should considerably surpass the performance of EBBS now in use.

Acknowledgements

We want to thank Drs. H. Pfeiffer and D. Kern (IBM) for making us aware at the conference of an existing high speed parallel-plate blanker which compensates to a certain extent for time-of-flight effects. (Kuo HP, Foster J, Haase W, Kelly J, Oliver BM. (1983). A high speed blanker for a 300 MHz lithography system, in: Proc. 10th Intl. Conf. on Electron and Ion Beam Science and Technology, R. Bakish (ed.) Electrochemical Soc. Inc., Pennington, NJ Vol. 1, 78-91).

References

[1] Feuerbaum HP. (1979). VLSI testing using the electron probe, Scanning Electron Microsc. 1979; I:285-296.

[2] Feuerbaum HP, Otto J. (1978). Beam chopper for subnanosecond pulses in scanning electron microscopy. Sci. Instr. 11, 529-532.

[3] Fujioka H, Ura K. (1983). Electron beam blanking systems. Scanning 5, 3-13.

[4] Gopinath A, Hill MS. (1977). Deflection beam chopping in SEM. J. Phys. E: Sci. Instr. 10, 229-236.

[5] Hawkes PW. (1983). Computer-aided calculation of the aberration coefficients of microwave cavity lenses. Optik 63, 129-156.

[6] Lischke B, Plies E, Schmitt R. (1983). Resolution limits in stroboscopic electron beam instruments, Scanning Electron Microsc. 1983; III:1177-1185.

[7] Lukianov AE, Spivak GV. (1966). Electron mirror microscopy of transient in semiconductor diodes, in: Proc. 6th Int. Cong. Electron Microsc. Kyoto, Vol. I, Maruzen Company Ltd., Tokyo,611-612.

[8] Menzel E, Kubalek E. (1979). Electron beam chopping systems in the SEM, Scanning Electron Microsc. 1979; I:305-318.

[9] Oldfield LC. (1976). A rotationally symmetric electron beam chopper for picosecond pulses. J. Phys. E: Sci. Instr. 9, 455-463.

[10] Plies E. (1982). Proposal for an electron beam blanking system with monochromator effect, in: Proc. 10th Int. Congr. Electron Microsc. Hamburg, Vol. I, Deutsche Gesellschaft für Elektronenmikroskopie,Frankfurt,319-320.

[11] Plows GS, Nixon WC. (1968). Stroboscopic scanning electron microscopy. J. Phys. E: Sci. Instr. 1, 595-600.

[12] Szentesi OI. (1972). Stroboscopic electron mirror microscopy at frequencies up to 100 MHz. J. Phys. E: Sci. Instr. 5, 563-567.

[13] Sturrock PA. (1955). Static and Dynamic Electron Optics, University Press, Cambridge, 148-185.

[14] Ura K, Fujioka H, Hosakawa T. (1978). Electron optical design of picosecond pulse stroboscopic SEM, Scanning Electron Microsc. 1978; I:747-753.

[15] Weinfeld M, Bouchoule A. (1976). Electron gun for generation of subnanosecond electron packets at very high repetition rate. Rev. Sci. Instr. 47, 412-417.